an energy-level diagram in an emitter conducive to observing forbidden transitions, even without outcoupling.

With regard to applications of this work to fundamental light-matter interactions, we believe that a number of fruitful extensions are within reach. Beyond the processes that we considered in this work, one can consider combinations of these processes, such as (i) multiplasmon transitions mediated by higher-order multipole virtual transitions, such as a two-plasmon emission with a total angular momentum change of 4 for the electron by way of intermediate quadrupole virtual transitions; (ii) third- and higher-order plasmon emission and absorption processes; or (iii) a second-order absorption process in which a plasmon and a far-field photon are absorbed, leading to large changes in energy and angular momentum of the electron due to the photon and plasmon, respectively.

All of these transitions should be enhanced using 2D plasmonics, but beyond the reach of conventional plasmonics and photonics without extremely high intensities of light. We stress that the results we have presented are not optimized. We performed our work with hydrogen purely as a proof-of-concept. For example, by finding an atom with a high octupole moment, it should be possible to make the octupole transition dominant over the dipole and other multipolar transitions, thereby paving the way for emitters with characteristic multipolarity different from dipolar. It should similarly be possible to optimize the rate of multiplasmon spontaneous emission relative to other transitions, leading to emitters highly capable of emitting entangled light.

Potential applications of this work include spectroscopy for inferring electronic transitions that cannot be determined with photons, sensors based on forbidden transitions, organic light sources arising from fast singlet-triplet transitions, fast entangled light generation, and fast generation of broadband light with tunable width in the near- and mid-infrared. Many of these applications could also be realized with the highly dissipative visible-frequency excitations in 2D conductors.

REFERENCES AND NOTES

1. P. A. Dirac, *Proc. R. Soc. London Ser. A* **114**, 243–265 (1927).
2. M. Pelton, *Nat. Photonics* **9**, 427–435 (2015).
3. M. Tame *et al.*, *Nat. Phys.* **9**, 329–340 (2013).
4. R. Friend *et al.*, *Nature* **397**, 121–128 (1999).
5. A. Köhler, H. Bässler, *Mater. Sci. Eng. Rep.* **66**, 71–109 (2009).
6. M. Göppert, *Naturwissenschaften* **17**, 932 (1929).
7. C. L. Cesar *et al.*, *Phys. Rev. Lett.* **77**, 255–258 (1996).
8. A. Hayat, P. Ginzburg, M. Orenstein, *Nat. Photonics* **2**, 238–241 (2008).
9. A. Nevet *et al.*, *Nano Lett.* **10**, 1848–1852 (2010).
10. A. Hayat, A. Nevet, P. Ginzburg, M. Orenstein, *Semicond. Sci. Technol.* **26**, 083001 (2011).
11. T. Nagao, T. Hildebrandt, M. Henzler, S. Hasegawa, *Phys. Rev. Lett.* **86**, 5747–5750 (2001).
12. B. Diaconescu *et al.*, *Nature* **448**, 57–59 (2007).
13. Y. Liu, R. Willis, K. Emtsev, T. Seyller, *Phys. Rev. B* **78**, 201403 (2008).
14. E. Rugeramigabo, T. Nagao, H. Pfnür, *Phys. Rev. B* **78**, 155402 (2008).
15. M. Jablan, H. Buljan, M. Soljačić, *Phys. Rev. B* **80**, 245435 (2009).
16. S. J. Park, R. E. Palmer, *Phys. Rev. Lett.* **105**, 016801 (2010).
17. A. Grigorenko, M. Polini, K. Novoselov, *Nat. Photonics* **6**, 749–758 (2012).
18. Z. Fei *et al.*, *Nature* **487**, 82–85 (2012).
19. M. Jablan, M. Soljačić, H. Buljan, *Proc. IEEE* **101**, 1689–1704 (2013).
20. K. Tielrooij *et al.*, *Nat. Phys.* **11**, 281–287 (2015).
21. A. Woessner *et al.*, *Nat. Mater.* **14**, 421–425 (2015).
22. Q. Zhang *et al.*, *Sci. Rep.* **4** 6559 (2014).
23. Z. Fei *et al.*, *Nano Lett.* **11**, 4701–4705 (2011).
24. H. Yan *et al.*, *Nat. Photonics* **7**, 394–399 (2013).
25. E. Altewischer, M. P. van Exter, J. P. Woerdman, *Nature* **418**, 304–306 (2002).
26. A. Archambault, F. Marquier, J.-J. Greffet, C. Arnold, *Phys. Rev. B* **82**, 035411 (2010).
27. F. H. Koppens, D. E. Chang, F. J. García de Abajo, *Nano Lett.* **11**, 3370–3377 (2011).
28. L. Gaudreau *et al.*, *Nano Lett.* **13**, 2030–2035 (2013).
29. See supplementary materials on *Science* Online.
30. We expect nonlocal effects to kick in at atom-surface separations $z_0 \leq v_f/\omega_0$, where v_f is the Fermi velocity and ω_0 is the transition frequency.
31. A. Kramida *et al.*, Atomic Spectra Database (National Institute of Standards and Technology, Gaithersburg, MD, 2012).
32. J. R. Zurita-Sánchez, L. Novotny, *J. Opt. Soc. Am. B* **19**, 1355 (2002).
33. J. R. Zurita-Sánchez, L. Novotny, *J. Opt. Soc. Am. B* **19**, 2722 (2002).
34. R. Filter, S. Mühlig, T. Eichelkraut, C. Rockstuhl, F. Lederer, *Phys. Rev. B* **86**, 035404 (2012).
35. M. Takase *et al.*, *Nat. Photonics* **7**, 550–554 (2013).
36. V. Yannopapas, E. Paspalakis, *J. Mod. Opt.* **62**, 1435–1441 (2015).
37. M. L. Andersen, S. Stobbe, A. S. Sørensen, P. Lodahl, *Nat. Phys.* **7**, 215–218 (2011).
38. I. D. Rukhlenko *et al.*, *Opt. Express* **17**, 17570–17581 (2009).
39. P. K. Jain, D. Ghosh, R. Baer, E. Rabani, A. P. Alivisatos, *Proc. Natl. Acad. Sci. U.S.A.* **109**, 8016–8019 (2012).
40. G. M. Akselrod *et al.*, *Nat. Photonics* **8**, 835–840 (2014).
41. Technically, $\nabla \cdot \mathbf{E} \neq 0$ only at the surface, but the contribution is small because the atomic wave functions are exponentially suppressed at the surface, so for parameters of interest, the direct s → s transition is much weaker than the two-plasmon process.
42. A. F. Page, F. Ballout, O. Hess, J. M. Hamm, *Phys. Rev. B* **91**, 075404 (2015).
43. A. Alabastri, X. Yang, A. Manjavacas, H. O. Everitt, P. Nordlander, *ACS Nano* **10**, 4835–4846 (2016).
44. G. Liu *et al.*, *ACS Nano* **6**, 6786–6792 (2012).
45. A. N. Abbas *et al.*, *ACS Nano* **8**, 1538–1546 (2014).
46. T. B. Hoang *et al.*, *Nat. Commun.* **6**, 7788 (2015).
47. For applications in which fast nonradiative decay is desired, we note that for considerably low wavelengths $1/kz_0 \approx 1$, the nonradiative decay is much faster than one would naively expect. This is because the nonradiative decay still couples to the multipole moment relevant to the atomic transition. Therefore, the strong enhancement of rates coming from matching the atomic size to the wavelength of light compensates for the suppression of rates coming from a higher kz_0. In fact, the total rate—even when nonradiative energy transfer is dominant—increases as the wavelength shrinks. From this, we conclude that for both radiative and nonradiative decay, the high confinement of 2D plasmons helps to overcome the small size of the atom.
48. C. Cohen-Tannoudji, J. Dupont-Roc, G. Grynberg, P. Thickstun, *Atom-Photon Interactions: Basic Processes and Applications* (Wiley, 1992).
49. We note that in principle the spectra increase for low frequencies because of quenching, but in the cases presented, it only provides a weak logarithmic correction to the decay rates (one to two orders of magnitude below the computed decay rates in Fig. 4F). This logarithmic correction is regulated by the energy difference between 4s and 4p levels (due to the Lamb shift). In other atoms, it is regulated by a much larger frequency (due to the lack of degeneracy between s and p orbitals), making the correction even weaker than in hydrogen (*29*).
50. A. Alù, N. Engheta, *Nat. Photonics* **2**, 307–310 (2008).

ACKNOWLEDGMENTS

Supported by S3TEC, an Energy Frontier Research Center funded by U.S. Department of Energy grant DE-SC0001299 (B.Z. and M.S.); Marie Curie grant 328853-MC-BSiCS (I.K.); and the Army Research Office through the Institute for Soldier Nanotechnologies under contract W911NF-13-D-0001. We thank P. Rebusco for critical reading and editing of the manuscript, and H. Buljan, K. Nelson, O. Shapira, and J. Lopez for useful discussions. The authors and MIT have filed U.S. patent applications 62/342,287 and 62/266,762 that relate to the mechanisms described in this manuscript.

SUPPLEMENTARY MATERIALS

www.sciencemag.org/content/353/6296/263/suppl/DC1
Figs. S1 to S5
References (*51*–*55*)

6 March 2016; accepted 17 June 2016
10.1126/science.aaf6308

OZONE HOLE

Emergence of healing in the Antarctic ozone layer

Susan Solomon,[1]* Diane J. Ivy,[1] Doug Kinnison,[2] Michael J. Mills,[2] Ryan R. Neely III,[3,4] Anja Schmidt[3]

Industrial chlorofluorocarbons that cause ozone depletion have been phased out under the Montreal Protocol. A chemically driven increase in polar ozone (or "healing") is expected in response to this historic agreement. Observations and model calculations together indicate that healing of the Antarctic ozone layer has now begun to occur during the month of September. Fingerprints of September healing since 2000 include (i) increases in ozone column amounts, (ii) changes in the vertical profile of ozone concentration, and (iii) decreases in the areal extent of the ozone hole. Along with chemistry, dynamical and temperature changes have contributed to the healing but could represent feedbacks to chemistry. Volcanic eruptions have episodically interfered with healing, particularly during 2015, when a record October ozone hole occurred after the Calbuco eruption.

Antarctic ozone depletion has been a focus of attention by scientists, policy-makers, and the public for three decades (*1*). The Antarctic ozone hole opens up in austral spring of each year and is measured both by its depth (typically a loss of about half of the total integrated column amount) and its extent (often more than 20 million km^2 by October). Ozone losses have also been documented in the Arctic and at mid-latitudes in both hemispheres (*2*). Concern

about ozone depletion prompted a worldwide phaseout of the production of anthropogenic halocarbons containing chlorine and bromine, which are known to be the primary sources of reactive halogens responsible for the depletion (*2*). The ozone layer is expected to recover in response, albeit very slowly, mainly because of the long atmospheric residence time of the halocarbons (*2*).

Ozone recovery involves multiple stages, starting with (i) a reduced rate of decline, followed by (ii) a leveling off of the depletion and (iii) an identifiable ozone increase that can be linked to halocarbon reductions (*2*, *3*). For simplicity, we refer to the third stage of recovery as "healing." All three stages of recovery have been documented in the upper stratosphere in mid- and low latitudes, albeit with uncertainties (*2*, *4*–*6*). Some studies provide evidence for all three recovery stages in ozone columns at mid-latitudes, despite dynamical variability (*7*). Although the first and second stages of recovery have also been well documented in the Arctic and Antarctica (*8*–*10*), a recent scientific assessment concluded that the emergence of the third stage had not been established by previous studies of the polar regions (*2*). Further, in October of 2015, the Antarctic ozone hole reached a record size (*11*), heightening questions about whether any signs of healing can be identified in either polar region.

Controls on polar ozone

Polar ozone depletion is driven by chlorine and bromine chemistry linked to anthropogenic halocarbon emissions (*2*, *12*). But ozone is not expected to heal in a monotonic fashion as halocarbon concentrations decrease because of confounding factors (such as meteorological changes) that induce variability from one year to another and could influence trends (*2*, *13*, *14*).

The exceptionally large ozone depletion in the polar regions compared with lower latitudes is related to polar stratospheric cloud (PSC) particles that form under cold conditions. These clouds drive heterogeneous chlorine and bromine chemistry that is sensitive to small changes in temperature (and hence to meteorological variability). A second, related factor is change in the transport of ozone and other chemicals caused by circulation or mixing changes (*2*). Further, some PSCs, as well as aerosol particles capable of driving similar chemistry, are increased in abundance when volcanic eruptions increase stratospheric sulfur. Volcanically driven increases in Antarctic ozone depletion were documented in the early 1990s after the 1991 eruption of Mount Pinatubo and are well simulated by models (*15*, *16*). Since about 2005, a series of smaller-magnitude volcanic eruptions has increased stratospheric particle abundances (*17*, *18*), but the impact of these on polar ozone recovery has not previously been estimated.

[1]Department of Earth, Atmospheric, and Planetary Sciences, Massachusetts Institute of Technology, Cambridge, MA 02139, USA. [2]Atmospheric Chemistry Observations and Modeling Laboratory, National Center for Atmospheric Research (NCAR), Post Office Box 3000, Boulder, CO 80305, USA. [3]School of Earth and Environment, University of Leeds, Leeds, UK. [4]National Centre for Atmospheric Science, University of Leeds, Leeds, UK.
***Corresponding author. Email: solos@mit.edu**

Observations and model test cases

We examined healing using balloon ozone data from the Syowa and South Pole stations. We also used total ozone column measurements from the South Pole station and the Solar Backscatter Ultra-Violet satellite (SBUV; we averaged SBUV data over the region from 63°S to the polar edge of coverage). The SBUV record has been carefully calibrated and compared with suborbital data (*19*). We also used the Total Ozone Mapping Spectrometer/Ozone Monitoring Instrument (TOMS/OMI) merged data set for analysis of the horizontal area of the ozone hole (*20*). Calibrated SBUV data are currently only available up to 2014, whereas the other records are available through 2015 (affecting the time intervals evaluated here). Model calculations were carried out with the Community Earth System Model 1 (CESM1) Whole Atmosphere Community Climate Model (WACCM), which is a fully coupled state-of-the-art interactive chemistry climate model (*21*). We used the specified dynamics option, SD-WACCM, in which meteorological fields including temperature and winds are derived from observations (*22*, *23*). The analysis fields allow the time-varying temperature-dependent chemistry that is important in polar ozone depletion to be simulated in detail. The model's ability to accurately represent polar ozone chemistry has recently been documented (*23*, *24*). Aerosol properties were based on the Chemistry and Climate Model Intercomparison (CCMI) recommendation (*25*) or derived inline from a version of WACCM that uses a modal aerosol submodel (*23*, *26*). The modal submodel calculates variations in stratospheric aerosols from volcanic sources (using an observational database of volcanic SO_2 emissions and plume altitudes; table S1) and nonvolcanic sulfur sources (particularly OCS, anthropogenic SO_2, and dimethyl sulfide). The injection heights and volcanic inputs are similar to those of previous studies (*18*, *27*), and the calculated aerosol distributions capture the timing of post-2005 eruptions observed in several low-, mid-, and high-latitude lidar data sets and satellite climatologies (*26*). Based on comparisons with lidar data for several eruptions and regions (*26*), our modeled post-2005 total stratospheric volcanic aerosol optical depths are estimated to be accurate to within ±40% (supplementary materials). Differences between the CCMI aerosol climatology and our calculated modal aerosol submodel results can be large, especially in the lower stratosphere (*26*), and can affect ozone abundances.

The concentrations of halogenated gases capable of depleting ozone stopped rising in the polar stratosphere around the late 1990s as a result of the Montreal Protocol and are slowly declining (*2*, *28*). We analyze what role these decreases in halogens play, along with other drivers of variability and change, in polar ozone trends since 2000. The year 2002 was anomalous in terms of meteorological behavior in the Antarctic (*29*), and it is excluded from all trend analyses throughout this paper.

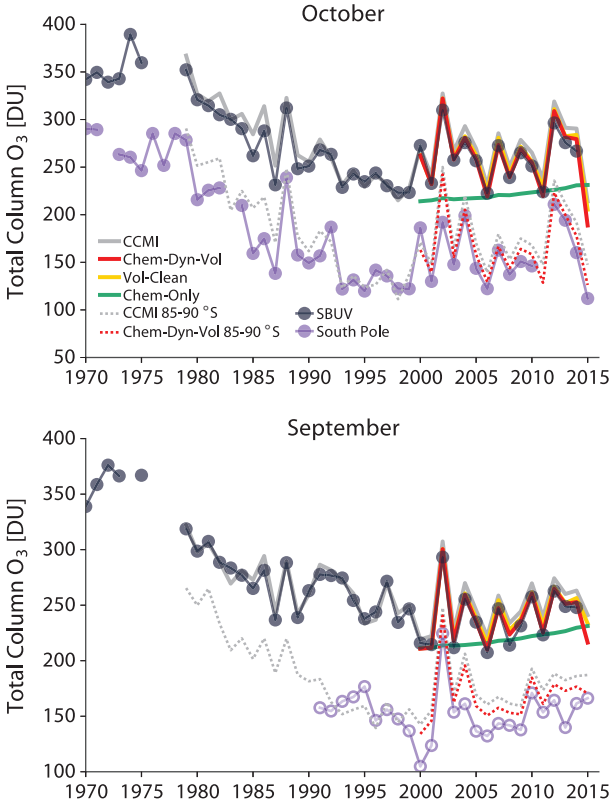

Fig. 1. Monthly averaged Antarctic total ozone column for October and September, from SBUV and South Pole station observations and a series of model calculations. Total ozone data measured at the geographic South Pole are from Dobson observations (filled circles) for October (**Top**) and balloon sondes (open circles) for September (**Bottom**), when there is not sufficient sunlight for the Dobson. SBUV data for each month are compared with model runs averaged over the polar cap latitude band that is accessible by the instrument; South Pole station data are compared with simulations for 85°S to 90°S.

Three different model simulations, all using full chlorine and bromine chemistry, were used to examine drivers of polar ozone changes since 2000: (i) a simulation encompassing observed time-varying changes in temperature and winds from meteorological analyses, with calculated background and volcanic stratospheric particles as well as other types of PSCs (chem-dyn-vol); (ii) a volcanically clean simulation (vol-clean), considering only background sources of stratospheric sulfur; and (iii) a chemistry-only simulation, in which annual changes in all meteorological factors (including the temperatures that drive chemistry) were suppressed by repeating conditions for 1999 throughout, and volcanically clean aerosols were imposed (chem-only). The Antarctic stratosphere in austral spring of 1999 was relatively cold and was deliberately chosen for the third simulation for its large chemical ozone losses. A longer run using full chemistry and CCMI aerosols illustrates the model's simulation of ozone loss since 1979. Further information on statistical approaches, methods, data sets, and the model are provided in the supplementary materials.

Our chem-only simulation probably represents a conservative estimate of chemical effects because it does not include radiatively driven temperature changes that are expected to occur as a result of changes in ozone (*30*) or the feedbacks of those temperature changes to chemical processes. Temperature and ozone are coupled because absorption of sunlight by ozone heats the stratosphere. If ozone increases as a result of reductions in halogens, then temperatures will increase, which feeds back to the chemistry (for example, by reducing the rate of temperature-dependent heterogeneous reactions that deplete ozone), further increasing ozone. Such effects have not been separated here from other changes in temperature or winds (due to dynamical variability or forcings such as greenhouse gases).

Antarctic ozone trends, variability, and fingerprints of healing

Most analyses of Antarctic ozone recovery to date consider October or September-to-November averages (*7*, *9*, *10*). The historic discovery of the Antarctic ozone hole was based on observations taken in October (*1*), and healing cannot be considered complete until the ozone hole ceases to occur in that month, which is expected around mid-century (*2*, *28*). However, October need not be the month when the onset of the healing process occurs. A first step in understanding whether a signal of the onset of healing can be identified is examining trends and their statistical significance relative to the noise of interannual variability.

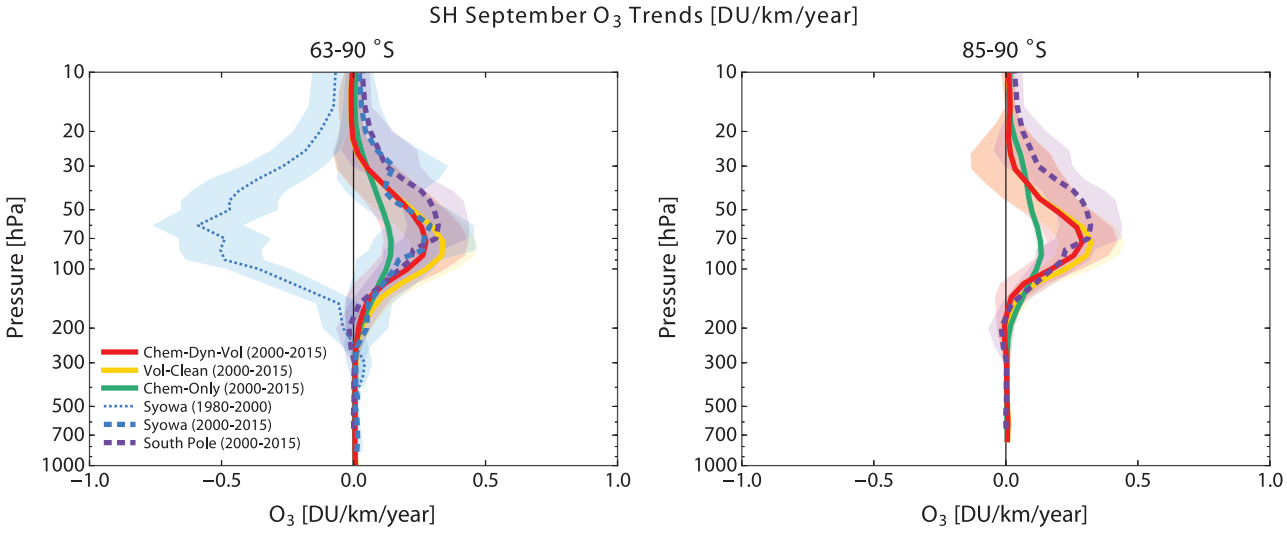

Fig. 2. Trends in Southern Hemisphere (SH) polar cap ozone profiles in September. Ozone data from balloons at the Syowa (69°S, 39.58°E) (**Left**) and South Pole (**Right**) stations, along with model simulations averaged over the polar cap and over 85°S to 90°S, respectively, are shown versus pressure. The shading represents the uncertainties on the trends at the 90% statistical confidence interval.

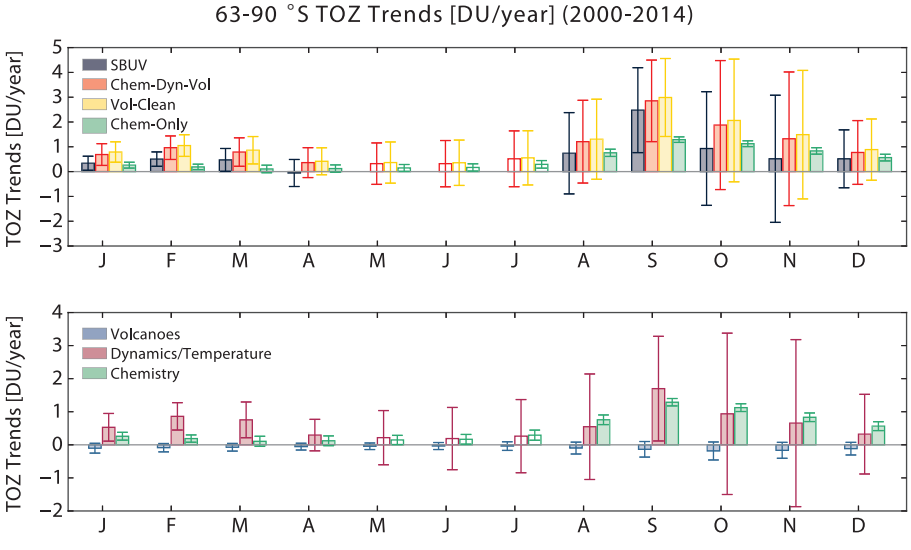

Fig. 3. Trends in total ozone abundance (TOZ) by month from 2000 to 2014. (**Top**) Monthly and polar cap–averaged SBUV satellite observations, together with model simulations masked to the satellite coverage. Error bars denote 90% statistical confidence intervals. (**Bottom**) Contributions to the simulated monthly trends in total ozone abundance driven by dynamics and temperature (vol-clean minus chem-only), chemistry only (chem-only), and volcanoes (chem-dyn-vol minus vol-clean). In austral winter, SBUV measurements do not extend to 63°S; therefore, the model averages for those months cover 63°S to 90°S (open bars).

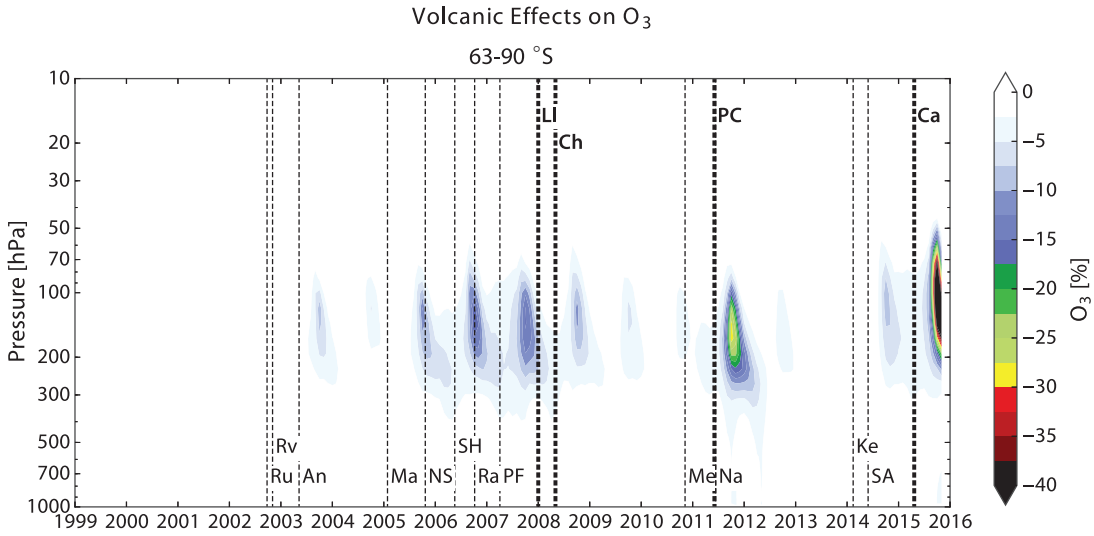

Fig. 4. Model-calculated percentage changes in local concentrations of ozone due to a series of moderate volcanic eruptions. The results (chem-dyn-vol minus vol-clean simulations) are averaged over the Antarctic polar cap as a function of pressure and month. Volcanic eruptions that have dominated the changes are indicated, with tropical eruptions at the bottom and higher-latitude eruptions at the top. An, Anatahan; Ca, Calbuco; Ch, Chaiten; Ke, Kelut; Ll, Llaima; Ma, Manam; Me, Merapi; Na, Nabro; NS, Negra Sierra; PC, Puyehue-Cordón Caulle; PF, Piton de la Fournaise; Ra, Rabaul (also referred to as Tavurvur); Ru, Ruang; Rv, Reventador; SA, Sangeang Api; SH, Soufriere Hills.

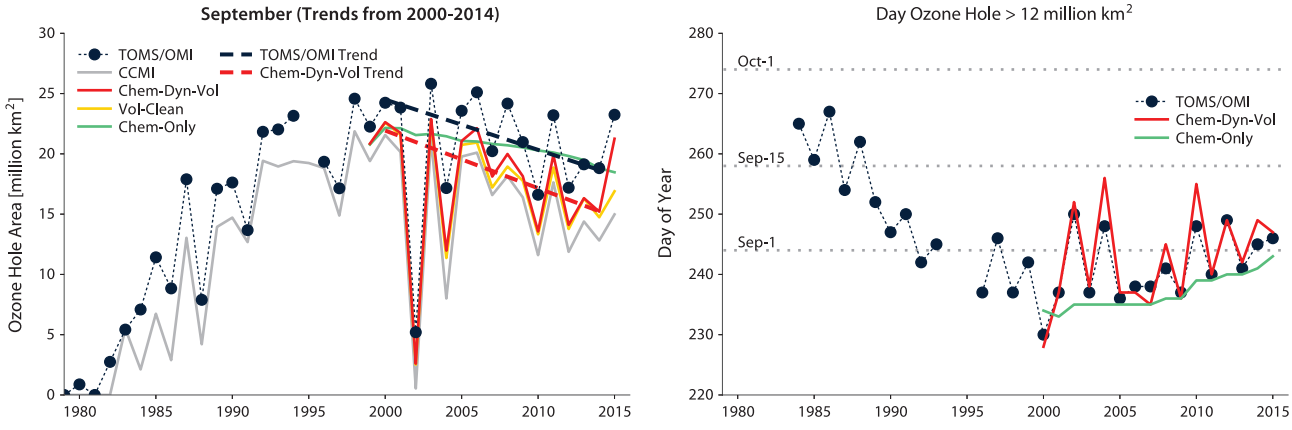

Fig. 5. September size of the ozone hole and day of year when the hole exceeds 12 million km^2 (**Left**) Annual size of the September monthly averaged ozone hole, defined as the region where the total ozone amount is less than 220 DU, from TOMS/OMI satellite observations and model simulations. Trends in the TOMS/OMI observations (heavy dashed black line) and the chem-dyn-vol model calculations (heavy dashed red line) from 2000 to 2015 are also indicated. (**Right**) Annual day of the year when the size of the ozone hole exceeds 12 million km^2 (and remains above that value for at least 3 days) in the TOMS/OMI observations and model simulations.

October has the deepest ozone depletion of any month in the Antarctic. However, it is subject to large variability due to seasonal fluctuations in temperature and transport, as well as to volcanic aerosol chemistry. Figure 1 shows the time series of measured Antarctic total ozone in October obtained from SBUV and South Pole station data, along with the model calculations; tables S2 and S3 provide the associated post-2000 trends and 90% confidence intervals. SD-WACCM reproduces the observed October variability from year to year when all factors are considered (chem-dyn-vol) (Fig. 1). However, the October total ozone trends are not yet positive with 90% certainty in the observational data or in the model. In contrast, other months with lower depletion and variability (particularly September; Fig. 1, fig. S1, and tables S2 and S3) reveal positive ozone trends from 2000 to 2014 that are statistically significant at 90% confidence in SBUV and South Pole station measurements. Arctic ozone has long been known to be more variable than Antarctic ozone (*2*), and no Arctic month yet reveals a significant positive trend in either the chem-dyn-vol simulation or the SBUV observations when examined in the same manner (table S2).

The September profile of balloon ozone trends is a key test of process understanding. Figure 2 shows measured balloon profile trends for the South Pole and Syowa stations for 2000–2015, together with SD-WACCM model simulations. The large ozone losses measured at Syowa as the ozone hole developed from 1980 to 2000 are also shown for comparison. Antarctic station data need to be interpreted with caution because of an observed long-term shift in the position of the Antarctic vortex that affects Syowa in particular in October; the South Pole station is, however, less influenced by this effect (*31*). The ozonesonde data sets suggest clear increases since 2000 between about 100 and 50 hPa (*10*). The chem-only simulation reproduces about half of the observed healing, with the remainder in this month being accounted for by dynamics and temperature. The simulations also suggest a negative contribution (offset to healing) due to volcanic enhancements of the ozone depletion chemistry between about 70 and 200 hPa (fig. S2 shows similar effects in other months in this sensitive height range). The comparisons of the modeled trend profiles in Fig. 2 provide an important fingerprint of the onset of healing of

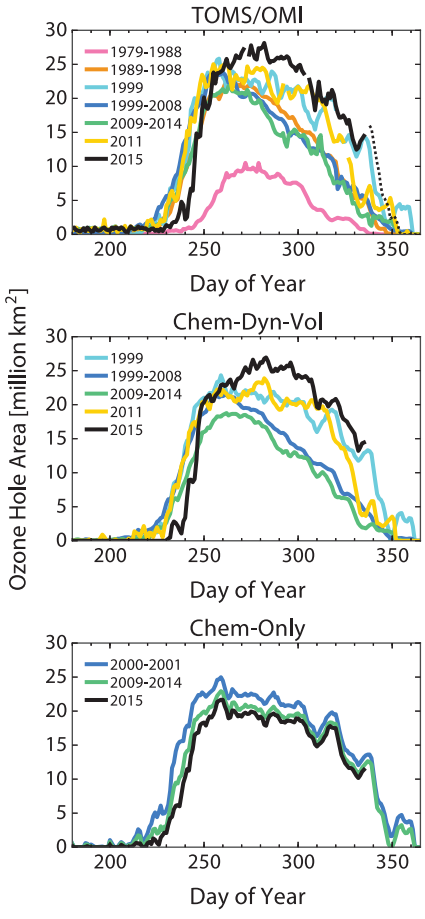

Fig. 6. Daily size of the ozone hole. Daily measurements (**Top**) and model calculations (**Middle** and **Bottom**) of the size of the Antarctic ozone hole versus day of year for different time intervals, with 2015 shown in black. The dashed black line in the top panel denotes the 2015 TOMS/OMI data after the period covered by the model runs.

the Antarctic ozone layer in September. This is consistent with the basic understanding that reductions in ozone-depleting substances in the troposphere will lead to a healing of polar ozone that emerges over time, with lags due to the transport time from the troposphere to the stratosphere, along with the time required for chemically driven trends to become significant relative to dynamical and volcanic variability.

The seasonal cycle of monthly total ozone trends from the SBUV satellite observations is shown in Fig. 3, along with model calculations for various cases. The contributions to the modeled trends that are due to volcanic inputs (difference between chem-dyn-vol and vol-clean simulations), chemistry alone (chem-only simulations), and dynamics and temperature (difference between vol-clean and chem-only simulations) are shown in the lower panel. Although it is not possible to be certain that the SBUV observations vary for the same reasons that the model calculations do, the broad agreement between them on the seasonal cycle of total trends supports this interpretation. Less dynamical variability in September compared with October (as shown by smaller error bars on the "dynamics/temperature" term in Fig. 3, bottom panel), along with strong chemical recovery, make September the month when the Antarctic ozone layer has undergone the largest amount of healing since 2000. The data suggest September increases (at 90% confidence) of 2.5 ± 1.6 DU per year over the latitudes sampled by SBUV and 2.5 ± 1.5 DU per year from the South Pole sondes. These values are consistent with the chem-dyn-vol model values of 2.8 ± 1.6 and 1.9 ± 1.5 DU per year, respectively. Because the model reproduces much of the observed year-to-year variability in September total ozone from both the South Pole station and SBUV observations, confidence is increased that there is a significant chemical contribution to the trends (Fig. 1). As a best estimate, the model results suggest that roughly half of the September column healing is chemical, and half is due to dynamics and temperature, though the dynamic and temperature effects are highly variable. The modeled total September healing trend has been reduced by about 10% as a result of the chemical effects of increased volcanic activity in the latter part of 2000–2014.

Volcanic eruptions affect polar ozone depletion because injections of sulfur increase the surface areas of liquid PSCs and aerosol particles (*32*). Higher-latitude eruptions directly influence the polar stratosphere, but tropical eruptions also can increase polar aerosols via transport. The model indicates that numerous moderate eruptions since about 2005 have affected polar ozone in both hemispheres (table S1 gives eruptions, dates, and latitudes), particularly at pressures from about 70 to 300 hPa (Fig. 4). At pressures above about 100 hPa, temperatures are generally too warm for many PSCs to form, but there is sufficient water that effective heterogeneous chemistry can take place under cold polar conditions (*12*). Our simulations indicate peak volcanic losses locally as large as 30 and 55% for the Antarctic in 2011 and 2015, mainly due to the Chilean eruptions of Puyehue-Cordón Caulle and Calbuco, respectively; contributions to depletions that are attributable to tropical eruptions are also evident in several earlier years. At these pressures, contributions to the total column are small but significant: The integrated additional Antarctic ozone column losses, averaged over the polar cap, are between 5 and 13 DU after the eruptions shown in Fig. 4.

The ozone hole typically begins to open in August of each year and reaches its maximum areal extent in October. Decreases in the areal extent of the October hole are expected to occur in the 21st century as chemical destruction slows, but they cannot yet be observed against the backdrop of interannual variability, in part because of the extremely large hole in 2015 (fig. S3). However, monthly averaged observations for September show a shrinkage of 4.5 ± 4.1 million km^2 between 2000 and 2015 (Fig. 5, left panel). The model underestimates the observed September hole size by about 15% on average, but it yields variability (Fig. 5) and trends (4.9 ± 4.7 million km^2) that are similar to the observations. The right panel of Fig. 5 shows that the observed and modeled day of the year when the ozone hole exceeds a threshold value of 12 million km^2 has been occurring later in recent years, indicating that early September holes are becoming smaller (Fig. 6). This result is robust to the specific choice of threshold value and implies that the hole is opening more slowly as the ozone layer heals. The chem-only simulation results in Fig. 5 show that if temperatures, dynamical conditions, and volcanic inputs had remained the same as they were in 1999 until now, the September ozone hole would have shrunk by about 3.5 ± 0.3 million km^2 as a result of reduced chlorine and bromine; thus, the reduction of these chemicals dominates the total shrinkage over this period.

Volcanic eruptions caused the modeled areas of the September-averaged ozone holes to expand substantially in several recent years. Our results, as shown in Fig. 5 (left panel), indicate that much of the statistical uncertainty in the observed September trend is not random, but rather is due to the expected chemical impacts of these geophysical events. In 2006, 2007, and 2008, model calculations suggest that the September ozone holes were volcanically enlarged by about 1 million km^2. The sizes of the September ozone holes in 2011 and 2015 are estimated to have been, respectively, about 1.0 million and 4.4 million km^2 larger because of volcanic eruptions (especially Puyehue-Cordón Caulle in 2011 and Calbuco in 2015) than they would otherwise have been, substantially offsetting the chemical healing in those years.

Figure 6 shows that the bulk of the seasonal growth of the ozone hole typically occurs between about days 230 and 250 (late August to early September). As the ozone layer heals, the growth of the hole is expected to occur later in the year (middle and bottom panels), in agreement with observations (top). The slower rates of early-season growth are key to the trend of shrinkage in the September-averaged ozone hole. For example, the rate of ozone loss depends strongly upon the ClO concentration, so that reduced chlorine concentrations lead to slower rates of ozone loss after polar sunrise. The ozone hole of 2015 was considerably larger over several weeks in October (but notably, not in September) than ever previously observed, and this behavior is well reproduced in our model only when the eruption of Calbuco is considered (figs. S3 and S4). The record-large monthly averaged ozone hole in October 2015 measured 25.3 million km^2, which is 4.8 million km^2 larger than the previous record year (20.6 million km^2 in 2011). When volcanic aerosols are included (chem-dyn-vol simulation), our calculated monthly averaged October 2015 ozone hole is 24.6 million km^2, whereas the corresponding value excluding volcanic aerosols (vol-clean simulation) is much smaller, 21.1 million km^2 (fig. S3). Therefore, our calculations indicate that cold temperatures and dynamics alone made a much smaller contribution to establishing the October 2015 record than volcanic aerosols did (figs. S3 and S4), and the cold temperatures are expected to be at least partly a feedback to the volcanically increased large ozone losses. Further, the conclusion that the volcanic aerosols were the dominant cause of the

record size of the October 2015 ozone hole would hold based on our calculations even if the volcanic aerosol amounts were overestimated by a factor of several (a much larger error than indicated by our comparison of our model calculations with lidar data for multiple eruptions in (*26*); supplementary materials).

The reasons for the contributions of dynamics and temperature to the healing of the Antarctic ozone layer are not clear. The dynamical and temperature contributions to healing estimated in Fig. 3 vary by month in a manner that mirrors the ozone depletion in spring, suggesting linkages to the seasonality of the depletion itself and hence possible dynamical feedbacks. Some models (*33*–*35*) suggest that a reduction in transport of ozone to the Antarctic occurred as depletion developed in the 1980s and 1990s, which would imply a reversal of this process and hence increased healing as ozone rebounds. But others indicate that ozone depletion increased the strength of the stratospheric overturning circulation (*36*), and a reversal of this factor during recovery would impede healing. Although there is robust agreement across models that climate change linked to increasing greenhouse gases should act to increase the strength of the stratospheric overturning circulation, observations show mixed results (*37*); further, the seasonality of this effect has not been established, and the magnitude in the Antarctic is uncertain. Internal variability of the climate system linked, for example, to variations in El Niño could also affect the trends.

Conclusion

After accounting for dynamics, temperature, and volcanic factors, the results presented here indicate that healing of the Antarctic ozone hole is emerging. Our results underscore the combined value of balloon and satellite ozone data, volcanic aerosol measurements, and chemistry-climate models in documenting progress in the recovery of the ozone layer since the Montreal Protocol.

REFERENCES AND NOTES

1. J. C. Farman, B. G. Gardiner, J. D. Shanklin, *Nature* **315**, 207–210 (1985).
2. World Meteorological Organization/United Nations Environment Programme (WMO/UNEP), *Scientific Assessment of Ozone Depletion: 2014* (Global Ozone Research and Monitoring Project Report No. 55, WMO, 2014).
3. D. J. Hofmann, S. J. Oltmans, J. M. Harris, B. J. Johnson, J. A. Lathrop, *J. Geophys. Res.* **102**, 8931–8943 (1997).
4. M. J. Newchurch *et al.*, *J. Geophys. Res.* **108**, 4507 (2003).
5. N. R. P. Harris *et al.*, *Atmos. Chem. Phys.* **15**, 9965–9982 (2015).
6. F. Tummon *et al.*, *Atmos. Chem. Phys.* **15**, 3021–3043 (2015).
7. T. G. Shepherd *et al.*, *Nat. Geosci.* **7**, 443–449 (2014).
8. E.-S. Yang *et al.*, *J. Geophys. Res.* **113**, D20308 (2008).
9. M. L. Salby, E. Titova, L. Deschamps, *Geophys. Res. Lett.* **38**, L09702 (2011).
10. J. Kuttippurath *et al.*, *Atmos. Chem. Phys.* **13**, 1625–1635 (2013).
11. WMO, "WMO Antarctic Ozone Bulletins: 2015," 2015; www.wmo.int/pages/prog/arep/WMOAntarcticOzoneBulletins2015.html.
12. S. Solomon, *Rev. Geophys.* **37**, 275–316 (1999).
13. J. Kuttippurath *et al.*, *Atmos. Chem. Phys.* **15**, 10385–10397 (2015).
14. N. J. Livesey, M. L. Santee, G. L. Manney, *Atmos. Chem. Phys.* **15**, 9945–9963 (2015).
15. D. J. Hofmann, S. J. Oltmans, *J. Geophys. Res.* **98**, 18555–18561 (1993).
16. R. W. Portmann *et al.*, *J. Geophys. Res.* **101**, 22991–23006 (1996).
17. J.-P. Vernier *et al.*, *Geophys. Res. Lett.* **38**, L12807 (2011).
18. C. Brühl, J. Lelieveld, H. Tost, M. Höpfner, N. Glatthor, *J. Geophys. Res. Atmos.* **120**, 2103–2118 (2015).
19. R. D. McPeters, P. K. Bhartia, D. Haffner, G. L. Labow, L. Flynn, *J. Geophys. Res.* **118**, 8032–8039 (2013).
20. W. Chehade, M. Weber, J. P. Burrows, *Atmos. Chem. Phys.* **14**, 7059–7074 (2014).
21. D. R. Marsh *et al.*, *J. Clim.* **26**, 7372–7391 (2013).
22. A. Kunz, L. L. Pan, P. Konopka, D. E. Kinnison, S. Tilmes, *J. Geophys. Res.* **116**, D24302 (2011).
23. Materials and methods are available as supplementary materials on *Science* Online.
24. S. Solomon, D. Kinnison, J. Bandoro, R. R. Garcia, *J. Geophys. Res.* **120**, 7958–7974 (2015).
25. F. Arfeuille *et al.*, *Atmos. Chem. Phys.* **13**, 11221–11234 (2013).
26. M. J. Mills *et al.*, *J. Geophys. Res.* **121**, 2332–2348 (2015).
27. M. Höpfner *et al.*, *Atmos. Chem. Phys.* **15**, 7017–7037 (2015).
28. P. A. Newman, E. R. Nash, S. R. Kawa, S. A. Montzka, S. M. Schauffler, *Geophys. Res. Lett.* **33**, L12814 (2006).
29. A. A. Scaife *et al.*, *J. Atmos. Sci.* **62**, 629–639 (2005).
30. P. M. Forster, R. S. Freckleton, K. P. Shine, *Clim. Dyn.* **13**, 547–560 (1997).
31. B. Hassler, G. E. Bodeker, S. Solomon, P. J. Young, *Geophys. Res. Lett.* **38**, L01805 (2011).
32. A. Tabazadeh, K. Drdla, M. R. Schoeberl, P. Hamill, O. B. Toon, *Proc. Natl. Acad. Sci. U.S.A.* **99**, 2609–2612 (2002).
33. S. Meul, S. Oberländer-Hayn, J. Abalichin, U. Langematz, *Atmos. Chem. Phys.* **15**, 6897–6911 (2015).
34. P. Braesicke *et al.*, *Atmos. Chem. Phys.* **13**, 10677–10688 (2013).
35. F. Li, J. Austin, J. Wilson, *J. Clim.* **21**, 40–57 (2008).
36. C. McLandress, T. G. Shepherd, *J. Clim.* **22**, 1516–1540 (2009).
37. N. Butchart, *Rev. Geophys.* **52**, 157–184 (2014).

ACKNOWLEDGMENTS

We thank S. Tilmes (NCAR) for help with the MERRA (Modern-Era Retrospective Analysis for Research and Applications) data. D.K. and S.S. were partially supported by NSF Frontiers in Earth System Dynamics grant OCE-1338814, and D.J.I. was supported by NSF Atmospheric Chemistry grant AGS-1539972. A.S. was supported by an Academic Research Fellowship from the University of Leeds, an NCAR visiting scientist grant, and Natural Environment Research Council grant NE/N006038/1. NCAR is sponsored by NSF. WACCM is a component of CESM, which is supported by NSF and the Office of Science of the U.S. Department of Energy. We are grateful to D. Fahey, B. Hassler, W. D. McKenna, and the anonymous reviewers for helpful comments. Instructions for access to data reported in this paper are given in the supplementary materials.

SUPPLEMENTARY MATERIALS

www.sciencemag.org/content/353/6296/269/suppl/DC1
Materials and Methods
Figs. S1 to S4
Tables S1 to S3
References (*38*–*44*)

6 December 2015; accepted 20 June 2016
Published online 30 June 2016
10.1126/science.aae0061

REPORTS

FERROELECTRICITY

Discovery of robust in-plane ferroelectricity in atomic-thick SnTe

Kai Chang,[1,2]* Junwei Liu,[3,1,2]* Haicheng Lin,[1,2] Na Wang,[1,2] Kun Zhao,[1,2] Anmin Zhang,[4] Feng Jin,[4] Yong Zhong,[1,2] Xiaopeng Hu,[1,2] Wenhui Duan,[1,2] Qingming Zhang,[4,5] Liang Fu,[3] Qi-Kun Xue,[1,2] Xi Chen,[1,2]† Shuai-Hua Ji[1,2,6]†

Stable ferroelectricity with high transition temperature in nanostructures is needed for miniaturizing ferroelectric devices. Here, we report the discovery of the stable in-plane spontaneous polarization in atomic-thick tin telluride (SnTe), down to a 1–unit cell (UC) limit. The ferroelectric transition temperature T_c of 1-UC SnTe film is greatly enhanced from the bulk value of 98 kelvin and reaches as high as 270 kelvin. Moreover, 2- to 4-UC SnTe films show robust ferroelectricity at room temperature. The interplay between semiconducting properties and ferroelectricity in this two-dimensional material may enable a wide range of applications in nonvolatile high-density memories, nanosensors, and electronics.

Two-dimensional (2D) materials exhibit a wide range of symmetry-breaking quantum phenomena such as crystalline order (*1*, *2*), superconductivity (*3*, *4*), magnetism (*5*, *6*), and charge-density wave (*7*, *8*), which persist in the limit of a single-unit-cell thickness. It has been comparatively more difficult to explore ferroelectricity in ultrathin films. For the perovskite ferroelectric materials, stable out-plane spontaneous polarization has been discovered in the thin films of few unit cells (UCs) thickness (*9*–*12*). Theoretical studies point out that the charge screening, chemical bonding, and misfit strain at the interface may play a role in stabilizing ferroelectric states (*13*–*18*). The transition temperature in those ultrathin films usually decreases as the thickness is reduced (*10*–*12*, *19*), which could be understood by the destabilization of ferroelectric states through depolarization fields. In contrast, the transition temperature of ferroelectric polymer film is nearly independent of thickness, indicating 2D behavior (*20*).

Here, we use the molecular beam epitaxial technique to prepare atomic-thick ferroelectric

Emergence of healing in the Antarctic ozone layer
Susan Solomon, Diane J. Ivy, Doug Kinnison, Michael J. Mills, Ryan R. Neely III and Anja Schmidt (June 30, 2016)
Science **353** (6296), 269-274. [doi: 10.1126/science.aae0061]
originally published online June 30, 2016

Editor's Summary

Turning the corner

The Antarctic ozone hole is finally showing signs of disappearing, nearly 30 years after the Montreal Protocol came into effect. The Montreal Protocol, an international treaty that phased out the production of many of the human-made compounds responsible for stratospheric ozone destruction, is widely considered to be the most important and successful international environmental agreement. For years, it has slowed the rate of stratospheric ozone depletion, and now there are signs that the ozone abundance over Antarctica has begun to increase. Solomon *et al*. present observational data and model results to illustrate the trends and diagnose their causes.

Science, this issue p. 269

Science (print ISSN 0036-8075; online ISSN 1095-9203) is published weekly, except the last week in December, by the American Association for the Advancement of Science, 1200 New York Avenue NW, Washington, DC 20005.